Article citation info:
RYMARCZYK T, KŁOSOWSKI G. Innovative methods of neural reconstruction for tomographic images in maintenance of tank industrial reactors. Eksploatacja i Niezawodnosc – Maintenance and Reliability 2019; 21 (2): 261–267, http://dx.doi.org/10.17531/ein.2019.2.10.

Tomasz RYMARCZYK
Grzegorz KŁOSOWSKI

INNOVATIVE METHODS OF NEURAL RECONSTRUCTION FOR TOMOGRAPHIC IMAGES IN MAINTENANCE OF TANK INDUSTRIAL REACTORS

NOWATORSKIE METODY NEURONOWEJ REKONSTRUKCJI OBRAZÓW TOMOGRAFICZNYCH W EKSPLOATACJI ZBIORNIKOWYCH REAKTORÓW PRZEMYSŁOWYCH*

The article presents an innovative concept of improving the monitoring and optimization of industrial processes. The developed method is based on a system of many separately trained neural networks, in which each network generates a single point of the output image. Thanks to the elastic net method, the implemented algorithm reduces the correlated and irrelevant variables from the input measurement vector, making it more resistant to the phenomenon of data noises. The advantage of the described solution over known non-invasive methods is to obtain a higher resolution of images dynamically appearing inside the reactor of artifacts (crystals or gas bubbles), which essentially contributes to the early detection of hazards and problems associated with the operation of industrial systems, and thus increases the efficiency of chemical process control.

Keywords: *electrical tomography, industrial processes, process control, neural networks, machine learning.*

W artykule przedstawiono nowatorską koncepcję usprawnienia monitoringu i optymalizacji procesów przemysłowych. Opracowana metoda bazuje na systemie osobno wytrenowanych wielu sieci neuronowych, w którym każda sieć generuje pojedynczy punkt obrazu wyjściowego. Dzięki zastosowaniu metody elastic net zaimplementowany algorytm redukuje z wejściowego wektora pomiarowego zmienne skorelowane i nieistotne, czyniąc go bardziej odpornym na zjawisko zaszumienia danych. Przewagą opisywanego rozwiązania nad znanymi metodami nieinwazyjnymi jest uzyskanie wyższej rozdzielczości obrazów dynamicznie pojawiających się wewnątrz reaktora artefaktów (kryształów lub pęcherzy gazowych), co zasadniczo przyczynia się do wczesnego wykrycia zagrożeń i problemów związanych z eksploatacją systemów przemysłowych, a tym samym zwiększa efektywność sterowania procesami chemicznymi.

Słowa kluczowe: *tomografia elektryczna, procesy przemysłowe, sterowanie procesami, sieci neuronowe, uczenie maszynowe.*

1. Introduction

Many chemical engineering products are created as a result of processes carried out using technological lines in which chemical reactors play a key role. A chemical reactor is a vessel adapted to carry out reactions taking place inside it. The purpose of industrial tank reactors is to ensure optimal economic parameters of chemical processes [18]. It can be achieved by the appropriate reactor design and by the skillful overlap of the three types of sub-processes occurring inside the reactor, namely the transfer of mass, momentum and heat. In this way, process control can be based on a dynamic selection of parameters such as: mixing intensity, temperature, pressure, substrate ratios and others. The presented research included reactors in which reactions take place between solid and liquid as well as gas and liquid. The tank reactor diagram is shown in Fig. 1.

The first type of reaction concerns the crystallization of solids in a liquid environment. It covers industrial processes of synthesis and purification of solid substances and changes in particle properties. The reactors in which crystallization occurs are used in many branches of the economy, including: chemical, food [9], metallurgy and waste utilization [27]. One of the monitoring systems tasks of such processes is to provide precise information on the quantity, size and location of crystals formed in the liquid in real time.

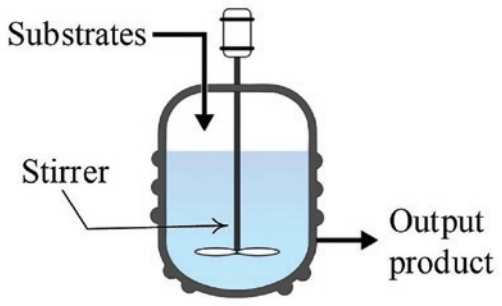

Fig. 1. Diagram of a tank reactor with a mixing system

The second type of reaction relates to the gas phase and the liquid phase. Such processes type are used, inter alia, in the production of biogas. Physicochemical fermentation reactors are a key element of biogas installations. Methane fermentation of organic waste takes place inside these reactors. The correct operation of technical systems is one of the crucial conditions for obtaining an adequate level of reliability of industrial processes [10].

There are two main reasons to monitor the state of dynamic processes. The first one is the detection of impending failures [11] which

(*) Tekst artykułu w polskiej wersji językowej dostępny w elektronicznym wydaniu kwartalnika na stronie ***www.ein.org.pl***

can include damage to technical infrastructure, excessive deviation of critical process parameters or interruption of its continuity. An effective monitoring system is designed to identify the problem early enough for effective corrective action to be taken.

The second reason for monitoring industrial processes is the need to control the course of the industrial process [29]. This is necessary for ensuring an adequate level of quality. In order to effectively control multiphase processes in which participate substances that can dynamically change the states of aggregation, effective monitoring methods should be applied. This is a difficult task, taking into account the aggressive conditions in which reactions take place inside the reactor. Using invasive sensors, the problem is the inability to directly examine any part of the interior of the reactor, point accuracy of measurements, the need to use many different monitoring systems simultaneously and high uncertainty in determining the dynamic state of the process based on incomplete data (indirect method). Among the non-invasive methods used in monitoring industrial processes can be distinguished: electric capacitive tomography [2, 4, 5, 13, 14, 16, 20, 26] electrical impedance tomography [3, 8, 28], magnetoacoustic tomography [30], ultrasound and radio tomography [21], X-ray tomography [1] and many more. Recently, more and more research in the field of industrial systems takes into account the use of various computational methods, such as: intelligent prediction methods [25], fuzzy logic [6], machine learning [22], numerical modeling [15], deep learning [8, 19] and binary programming [12].

Currently used techniques of non-invasive monitoring of industrial processes do not fully meet current operational needs. Obtained mapping of images of studied phenomena and processes can be unsharp, ambiguous, difficult to interpret, burdened with inaccuracies both in terms of the number of artefacts (crystals or gas bubbles) detected in the reactor as well as their size and location. As a result, redundant systems are used to obtain precise information about the status of the monitored process, which significantly increases the operating costs.

The above-mentioned difficulties and imperfections of the monitoring methods of chemical tank reactors are the reason for their improvement. The use of an improved monitoring method will increase the reliability of processes occurring inside the reactors and will reduce the operating costs of industrial systems.

The aim of this study is to introduce an improved method of monitoring and optimization of chemical processes occurring in heterogeneous tank reactors in which reactions take place between solid and liquid as well as gas and liquid. The applied method concerns electrical tomography [22]. The innovation is an original method of parallel use of a hybrid system that is a combination of the elastic net method and artificial neural networks [7, 23]. An advantage of the described concept over other known non-invasive methods is increased resistance to interference during measurements, higher accuracy of reconstruction, unlimited imaging resolution, low cost and high speed of operation. The description of the multiply neural system enabling effective monitoring of chemical reactions using electrical tomography is presented in the further part of this study.

Fig. 2. The test stand: a) hybrid tomograph, b) reactor with connected electrodes

a)

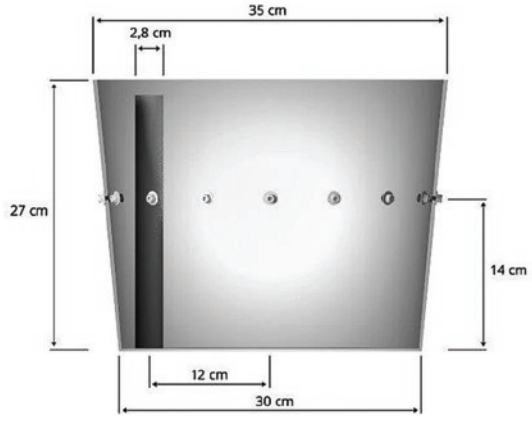

b)

Fig. 3. The physical EIT model with the electrodes: a) schematic drawing, b) reactor with artifacts immersed in liquid electrodes

2. Models, methods, algorithms

Electrical impedance tomography (EIT), like as electrical capacitance tomography (ECT), are non-invasive diagnostic methods of technical objects [15, 22]. The EIT method used in the described studies processes data generated by a system of 16 electrodes installed on the surface of the reactor. Fig. 2 and 3 present a research position with a physical model with an electrode system and a hybrid tomograph adapted for EIT measurements.

Fig. 4 presents the method of measuring the voltages generated by the arrangement of 16 electrodes. Due to the unknown value of voltage drops between the tested object and the electrodes to which the electric current source (I) is connected, these electrodes are not taken into account during the measurements. For each projection angle 12 independent voltage measurements (V) can be obtained between individual pairs of adjacent electrodes. This number results from the following calculation: n-4 = 12, where n = 16 is the total number of electrodes in the system, while 4 is the number of electrodes excluded from measurements within the projection angle. In this way, the total number of measurements is $(n-4)(n/2)=12\times 8=96$.

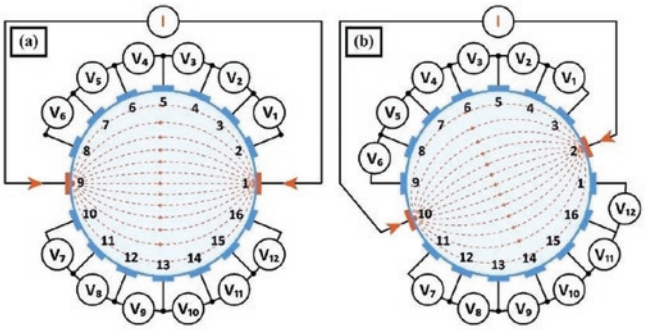

Fig. 4. The method of voltage measurement in a system of 16 electrodes: a) first measuring cycle, b) next measurement cycle

2.1. Hybrid neural algorithm

Dynamic progress in the field of low-cost technological solutions and access to advanced computational methods cause that the costs of using computing power and storage media are falling [16]. The popularity of computational techniques using parallel computations and requiring the processing of large data sets is growing [3]. As a result, there are less and less frequent situations in which researchers and designers of tomographic systems are forced to shorten the calculation time at the cost of the quality of results [17]. The presented tomographic system converts a vector of 96 voltages into an image with a resolution of 2883 pixels. Because the designed algorithm uses 2883 parallel-acting multiply neural networks, computing power is an important factor determining the speed of the measurement system. Fig. 5 shows the model of one of the 2883 hybrid subsystems to generate the actual value of a single point of the reconstructed image.

The algorithm for training a hybrid multiply neural system has the following sequence:

1. set-up the initial conditions:
   a) number of pixels in the mesh of the output image: m=2883;
   b) the size of the measurement vector $\boldsymbol{X_n}$ for each of the reconstructions: n=96;
   c) the number of cases that is required for neural networks training: N=99900;
   d) neural networks structure: $\tilde{n}_\upsilon$ -10-1, where $\tilde{n}_\upsilon$ means the reduced by the elastic net number of measurements at the input of the neural network generating υ-th pixel, 10 neurons in the hidden layer and 1 neuron in the output layer. Logistic transfer functions were used in both layers;
2. using the elastic net method, generate a matrix of individually reduced measurement vectors for each pixel of the output image separately:
   $\boldsymbol{X_n} \rightarrow elastic\,net \rightarrow \boldsymbol{X}_{\tilde{n},\upsilon}$, where $n=96$, $n>\tilde{n}>0$. You can use a subset with a number of cases much smaller than N, for example, 3000 randomly selected cases from the training set;
3. for υ=1 to m train neural network ANN_υ using the training set of the cardinality N;
4. save trained 2883 neural networks to the structural variable.

The mentioned above algorithm was implemented using the Matlab code, while the grid of the output image was modeled using the Eidors toolbox. Table 1 presents the results of the training process of one of 2883 neural networks, generating a real number determining the color of an example pixel on a tomographic image mesh. The pixel 600 was randomly chosen for the following test. Input data are included in the matrix $\boldsymbol{X_n}$ with dimensions of 96x99900 (96 measurements, 99900 cases). The input file was a vector $\boldsymbol{Y_\upsilon}$ with dimensions of 1x99900 (a single pixel of the image υ = 600, 99900 cases). Before training the network, the input vector was reduced from $n=96$ to $\tilde{n}=30$ using the elastic net method. The structure of the single neural network for point 600 was therefore: ANN_{600} = 30-10-1.

Table 1. The results of the training process along with the division of data

Division of the data set	The number of cases in a given set	Mean Square Error (MSE)	Regression (R)
1	2	3	4
Training set (70%)	69930	$7.65053\cdot10^{-3}$	0.813877
Validating set (15%)	14985	$7.27605\cdot10^{-3}$	0.806954
Testing set (15%)	14985	$8.27152\cdot10^{-3}$	0.822387

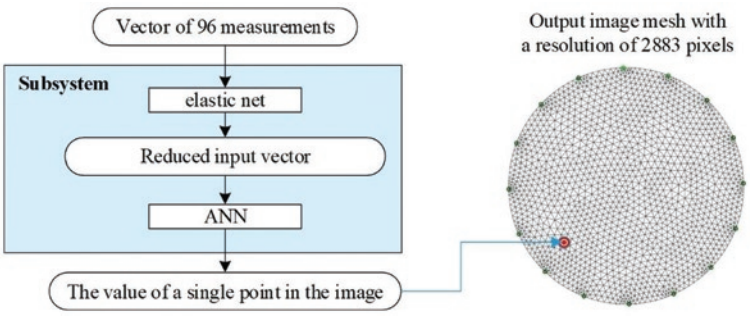

Fig. 5. The model of one of 2883 subsystems generating a single point of the image

A simulated collection of 99900 data have been divided into 3 parts: training, validating and testing in proportions 70/15/15, which is reflected in the first two columns of Table 1. Columns 3 and 4 contain information about error MSE and regression R for all 3 subsets that have been used in the network learning

process. The low value of MSE and R value close to 1 testify to the good quality of the trained network.

Formula (1) presents the method of calculating MSE:

$$MSE = \frac{1}{n}\sum_{i=1}^{n}\left(y_i' - y^*_i\right)^2 \quad (1)$$

where: n – image resolution; y_i' – the reference value of the i-th pixel; y^*_i – the reconstructive value of the i-th pixel.

The method of calculating the regression coefficient R is the formula (2):

$$R\left(y', y^*\right) = \frac{cov\left(y', y^*\right)}{\sigma_{y'}\sigma_{y^*}} \quad (2)$$

where: $\sigma_{y'}$ – standard deviation of reference values, σ_{y^*} – standard deviation of reconstructed values.

Fig. 6a shows the training progress of the selected ANN. The homogeneous hyperbolic shape of the graph line indicates that the network has not been overtrained. The lack of fluctuations and line compliance for all 3 data sets (learning, validation and test) indicates lack of overfitting and the network's ability to generalize. The graph also shows the moment when network learning process stopped. It happened after the 53-th epoch, when the MSE of the validating set reached the value of 0.0072761. The same value can also be read from column 3 of Table 1. The validating set was used to determine the condition of stop training ANN. This condition is met if the MSE of validation set does not decrease for 6 successive epochs.

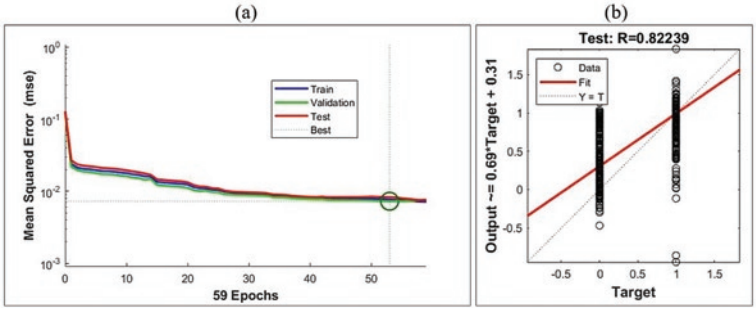

Fig. 6. Training process results for the selected network: a) MSE charts for the training, validating and testing set, b) regression statistics for the testing set

Information on the trained network is supplemented by Fig. 6b, which shows the graph of regression statistics for the testing set. The testing set gives the most reliable results regarding the quality of the received network, because the data contained therein did not have any impact on the learning process. As you can see, R = 0.82239 is consistent with the information from Table 1 contained in the bottom row of column 4. The characteristic way of data distribution in Fig. 6b results from the fact that the reference output image reflects only 2 values: 1 for background color and 0 for artifact (crystals or gas bubbles).

2.2. Improving the quality of measurement data using the elastic net

In the case of reconstruction of tomographic images of real objects with relatively low conductivity, the data from the electrodes are usually noisy. This is the result of the imperfection of electrode insulation, the effects of fast-changing and low currents generated by multiplexers, the influence of electromagnetic fields and many other factors. An example of technical facilities, from which tomographic data show a high level of noise are also industrial chemical reactors [18]. Disturbances of electrical signals are one of the main barriers hindering the development of tomographic methods for such objects [23].

To make the input data resistant to distortions and noise, the elastic net regularization was used [22]. In this method, we assume a certain linear system that can be described by means of the state equation (3):

$$Y = X\beta + \varepsilon \quad (3)$$

where $Y \in R^n$ is a matrix of output variables (reconstruction), $X \in R^{n\times(k+1)}$ represents the matrix of input variables, the coefficient $\beta \in R^{k+1}$ means a vector with unknown parameters, and $\varepsilon \in R^n$ reflects the sequence interference. If the linear task (4) has a solution in which the regression line intersects the y axis, then the first column of the matrix X in the linear equation (3) is a unitary column vector.

In the case when the predictors introduced into the regression model are strongly correlated with each other, a possible way to determine linear regression is to solve the problem (4):

$$\min_{(\beta_0,\beta')\in R^{k+1}} \frac{1}{2n}\sum_{i=1}^{n}\left(y_i - \beta_0 - x_i\beta'\right)^2 + \lambda P_\alpha\left(\beta'\right) \quad (4)$$

where: $x_i = \left(x_{i1},\ldots,x_{ik}\right)$, $\beta' = \left(\beta_1,\ldots,\beta_k\right)$ dla $1 \le i \le n$

P_α – elastic net penalty function is defined by the equation (3):

$$P_\alpha\left(\beta'\right) = \left(1-\alpha\right)\frac{1}{2}\left\|\beta'\right\|_{L_2} + \alpha\left\|\beta'\right\|_{L_1} = \sum_{j=1}^{k}\left(\frac{1-\alpha}{2}\beta_j^2 + \alpha\left|\beta_j\right|\right) \quad (5)$$

It can be seen that the penalty in this case is a linear combination of the L_1 and L_2 norms from unknown β' parameters. The introduction of the parameter-dependent penalties function to the objective function reduces the predictions of unknown parameters. The parameter λ in the task (5) represents the penalty factor. Entering the $0 \le \alpha \le 1$ parameter causes the task (4) to compromise between Lasso (least absolute shrinkage and selection operator) and ridge regression. If $\alpha = 0$ we deal with pure ridge regression called Tikhonov regularization. Ridge regression is a popular method of regularization of linear models [22].

If $\alpha = 1$ there is a pure Lasso method in task (4). Lasso is a statistical method that allows selection of independent variables

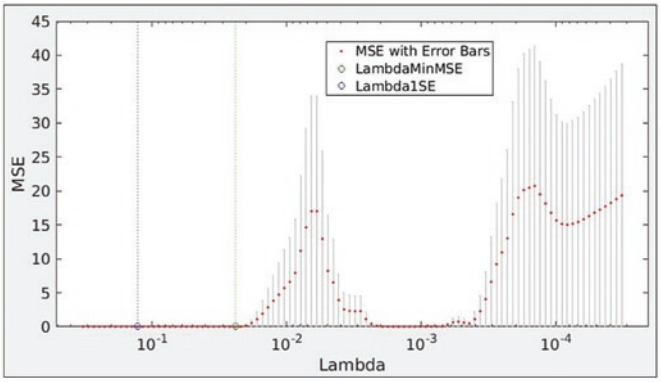

Fig. 7. Selection of Lambda parameter in the elastic net method with α = 0.25 based on the minimum mean square error (MSE)

and regularization of linear models. In the case of ridge regression, the coefficient of penalties is calculated in the L_1 norm and for Lasso in L_2 norm. Lasso is also indifferent to the correlation of predictors.

Figure 7 presents the process of selecting the parameter λ (lambda) in the elastic net method with the assumed α = 0.25 for one of the pixels of the output image. Two lambda values are marked with a green and blue dotted lines. The green line indicates the lambda value with the minimum mean square error (MSE) obtained using the cross-validation. This value has been marked with the LambdaMinMSE variable. The blue dotted line indicates the largest Lambda value, which is within the standard deviation of the minimum MSE (Lambda1SE). This lambda value means that even the worst of the tested models (with the largest MSE) still has a relatively low error value. In the described case λ = 0.129 for MSE = 0.0154 was assumed. The measurement vector has 96 values of voltage drops. In the considered case, thanks to the use of elastic net, the input vector has been reduced from 96 to 30 measurements.

3. Results

Fig. 8 presents a comparison of tomographic images obtained with two methods: ANN and a hybrid method combining elastic net with ANN.

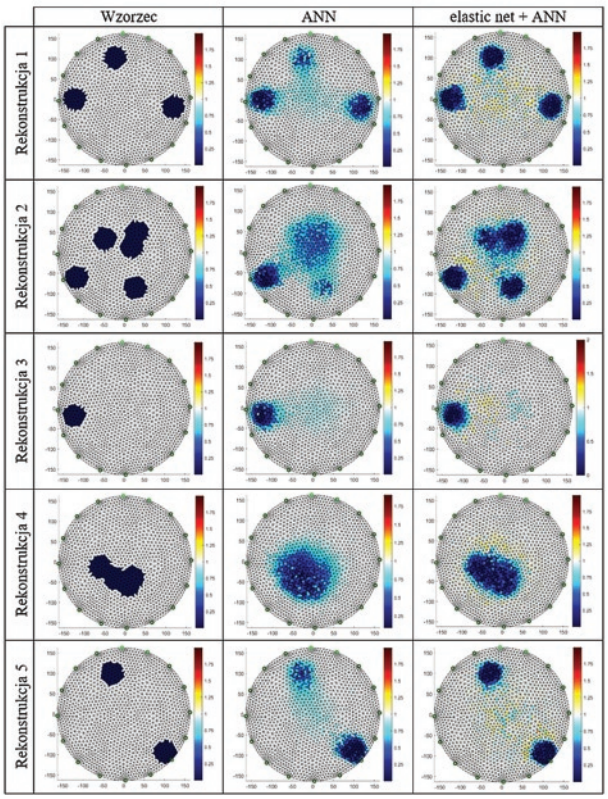

Fig. 8. Comparison of reconstructive images for ANN methods and "elastic net + ANN"

The first column contains reference images for the five tested cases. The test stand was calibrated in such a way that the value in the output, corresponding to the conductance of the reference liquid (water) equals 1. The values of the image pixels corresponding to the artefacts is 0. Next, using the physical model, real measurements were made by the ANN and elastic net + ANN (hybrid algorithm).

By comparing the images obtained with two methods, it can be noticed that in the hybrid approach, despite the reduction of the input measurement vector by almost 70% for each neural network, the visual quality of reconstruction is not worse than for pure ANN. It should also be noted that the algorithm reconstructs the worst artifacts located near the center of the reactor. This is most likely related to the distance of the recognized objects from the electrodes. Better reconstructions are obtained for artifacts that are localized closer to the electrodes.

Visual evaluation of reconstruction is not precise and insufficient for an objective comparison of the two analyzed methods. For this reason, three quantitative imaging quality indicators were introduced: MSE (Mean Squared Error), RIE (Relative Image Error) and ICC (Image Correlation Coefficient).

The relative RIE imaging error is calculated according to the formula (6):

$$RIE = \frac{\left\| Y^* - Y' \right\|}{\left\| Y' \right\|} \tag{6}$$

where: Y' – probability distribution of the pattern image pixels; Y^* – values of reconstructed pixels.

Formula (7) shows how to calculate the ICC image correlation coefficient:

$$ICC = \frac{\sum_{i=1}^{l} \left(y_i^* - \bar{Y}^* \right) \left(y_i' - \bar{Y}' \right)}{\sqrt{\sum_{i=1}^{l} \left(y_i^* - \bar{Y}^* \right)^2 \sum_{i=1}^{l} \left(y_i' - \bar{Y}' \right)^2}} \tag{7}$$

where: $\bar{Y}'$ – average probability distribution of the pattern image pixels; $\bar{Y}^*$ – average value of reconstructed pixels.

The smaller are the values of MSE and RIE coefficients, the better is the reconstruction quality. In the case of ICC, the opposite is true - the closer 1, the better the correlation of the output image with the reference image, which means a more accurate reconstruction.

Table 2 contains a summary of all three reconstruction quality indicators divided into tested methods and cases. The upper part of the table contains precisely calculated MSE, RIE and ICC values. In the right-hand column there are averaged values giving the possibility to make a generalized assessment of all five cases with one indicator. In order to facilitate the choice of the better method, the bottom part of the table contains a boolean classification of all indicators. Three questions have been formulated in such a way that in the case of an affirmative answer ("truth") a better method is "elastic net + ANN". In the case of a negative response ("false"), the index would prefer the pure ANN method.

As can be seen from Table 2, in all 18 cases, including responses and average values, the hybrid method „elastic net + ANN" turned out to be better.

4. Discussion and conclusions

The paper presents the results of research on the development of an improved algorithm for the reconstruction of images in the field of process tomography. In particular, the focus has been placed on imaging the cross-section of industrial tank reactors in which the processes of crystallization and anaerobic digestion occur in biogas installations. To make an objective assessment of the quality of the hybrid algorithm (elastic net + ANN), comparative studies were carried out using the physical laboratory model. Equal cases of artifact systems were prepared, and then voltage drops were read from the electrode system. Due to the fact that while reading data, many current-voltage states are transient, the data contained a certain level of noise. Af-

Table 2. Comparison of reconstruction indicators

Quality indicator of reconstruction		Number of reconstruction					Mean
		1	2	3	4	5	
ANN	MSE	0.0232	0.0573	0.0061	0.0337	0.0198	0.0280
	RIE	0.1587	0.2547	0.0795	0.1913	0.1451	0.1658
	ICC	0.8319	0.6715	0.8694	0.7301	0.7982	0.7802
elastic net + ANN	MSE	0.0158	0.0388	0.0047	0.0238	0.0115	0.0189
	RIE	0.1312	0.2096	0.0695	0.1610	0.1107	0.1364
	ICC	0.8804	0.7892	0.8987	0.8177	0.8907	0.8553
Is the MSE of the hybrid algorithm smaller than the MSE of pure ANN?		TRUE	TRUE	TRUE	TRUE	TRUE	TRUE
Is the RIE hybrid algorithm smaller than RIE of pure ANN?		TRUE	TRUE	TRUE	TRUE	TRUE	TRUE
Is the ICC of the hybrid algorithm greater than the ICC of pure ANN?		TRUE	TRUE	TRUE	TRUE	TRUE	TRUE

ter filtering the data using the background reference values (reactor without artefacts) obtained results were illustrated and converted into quality indicators: MSE, RIE and ICC.

Normally, if the clear measurement data used for the imaging were simulated and did not contain interference, removing 70% of the predictors (eg, reduction from 96 to 30) would result in poor image quality. The carried out experiments showed that it was different in the case of data with a certain level of noise. Although the obtained reconstructions, both for pure ANN and for the hybrid method, are still not perfect, they are nevertheless sufficiently accurate to determine the amount, shape and location of the artifacts. The time of reconstruction in all investigated cases with the Intel Core i7 processor machine did not exceed 1 second. This means that the developed algorithm can also be used in processes with high reaction dynamics and even in flow systems [24].

It is significant that in Table 2, in all cases tested and for all three quality indicators, better results were obtained using the "elastic net + ANN" algorithm, not pure ANN. It turns out that the application of elastic net caused that along with the removal of 70% of input variables, a lot of noisy data was deleted, generating various types of disturbances in the output image. This fact is proof that the newly developed hybrid algorithm "cleanses" the data and makes the tomographic system immune to various types of interference and noisy data.

The results of the research have proved that the use of the described solution enables a higher resolution of images of crystals or gas bubbles appearing inside the reactor, which essentially contributes to the early detection of hazards and facilitates solving the operational problems of industrial systems.

Acknowledgements

the authors would like to thank the authorities and employees of the Faculty of Mathematics, Physics and Computer Science of UMCS in Lublin for sharing supercomputing resources.

References

1. Babout L, Grudzień K, Wiącek J, Niedostatkiewicz M, Karpiński B, Szkodo M. Selection of Material for X-Ray Tomography Analysis and DEM Simulations: Comparison between Granular Materials of Biological and Non-Biological Origins. Granular Matter 2018; 20 (3): 38, https://doi.org/10.1007/s10035-018-0809-y.
2. Banasiak R, Wajman R, Sankowski D, Soleimani M. Three-Dimensional Nonlinear Inversion of Electrical Capacitance Tomography Data Using a Complete Sensor Model. Progress In Electromagnetics Research (PIER) 2010; 100: 219-234, https://doi.org/10.2528/PIER09111201.
3. Dusek J, Hladky D, Mikulka J. Electrical Impedance Tomography Methods and Algorithms Processed with a GPU. Progress In Electromagnetics Research Symposium - Spring (PIERS) 2017; 1710–14, https://doi.org/10.1109/PIERS.2017.8262025.
4. Garbaa H, Jackowska-Strumiłło L, Grudzień K, Romanowski A. Application of Electrical Capacitance Tomography and Artificial Neural Networks to Rapid Estimation of Cylindrical Shape Parameters of Industrial Flow Structure. Archives of Electrical Engineering 2016; 65 (4): 657–69, https://doi.org/10.1515/aee-2016-0046.
5. Grudzien K, Chaniecki Z, Romanowski A, Sankowski D, Nowakowski J, Niedostatkiewicz M. Application of Twin-Plane ECT Sensor for Identification of the Internal Imperfections inside Concrete Beams. IEEE International Instrumentation and Measurement Technology Conference Proceedings 2016; May, 1–6, https://doi.org/10.1109/I2MTC.2016.7520512.
6. Kłosowski G, Gola A, Świć A. Application of Fuzzy Logic Controller for Machine Load Balancing in Discrete Manufacturing System. In International Conference on Intelligent Data Engineering and Automated Learning 2015; 256–63, https://doi.org/10.1007/978-3-319-24834-9_31.
7. Kłosowski G, Rymarczyk T, Gola A. Increasing the Reliability of Flood Embankments with Neural Imaging Method. Applied Sciences 2018; 8 (9): 1457, https://doi.org/10.3390/app8091457.
8. Kłosowski G, Rymarczyk T. Using neural networks and deep learning algorithms in electrical impedance tomography. Informatyka Automatyka Pomiary w Gospodarce i Ochronie Środowiska 2017; 7 (3): 99–102, https://doi.org/10.5604/01.3001.0010.5226.

9. Korzeniewska E, Gałązka-Czarnecka I, Czarnecki A, Piekarska A, Krawczyk A. Influence of PEF on Antocyjans in Wine. Przegląd Elektrotechniczny 2018; 1 (1): 59–62, https://doi.org/10.15199/48.2018.01.15.
10. Korzeniewska E, Walczak M, Rymaszewski J. Elements of Elastic Electronics Created on Textile Substrate, Proceedings of the 24th International Conference Mixed Design of Integrated Circuits and Systems - MIXDES 2017; 2017, 447-45, https://doi.org/10.23919/MIXDES.2017.8005250.
11. Kosicka E, Kozłowski E, Mazurkiewicz D. Intelligent Systems of Forecasting the Failure of Machinery Park and Supporting Fulfilment of Orders of Spare Parts. In: Burduk A., Mazurkiewicz D. (eds) Intelligent Systems in Production Engineering and Maintenance – ISPEM 2017. ISPEM 2017. Advances in Intelligent Systems and Computing, vol 637. Springer, Cham, 2018, https://doi.org/10.1007/978-3-319-64465-3_6.
12. Kozłowski E., Mazurkiewicz D., Kowalska B., Kowalski, D. Binary Linear Programming as a Decision-Making Aid for Water Intake Operators. In: Burduk A., Mazurkiewicz D. (eds) Intelligent Systems in Production Engineering and Maintenance – ISPEM 2017. ISPEM 2017. Advances in Intelligent Systems and Computing, vol 637. Springer, Cham, 2018, https://doi.org/10.1007/978-3-319-64465-3_20.
13. Kryszyn J, Smolik W T, Radzik B, Olszewski T, Szabatin R. Switchless Charge-Discharge Circuit for Electrical Capacitance Tomography. Measurement Science and Technology 2014; 25 (11): 115009, https://doi.org/10.1088/0957-0233/25/11/115009.
14. Kryszyn J, Waldemar S. Toolbox for 3d Modelling and Image Reconstruction in Electrical Capacitance Tomography. Informatics Control Measurement in Economy and Environment Protection 2017; 7 (1).
15. Lopato P, Tomasz C, Sikora R, Gratkowski S, Ziolkowski M. Full Wave Numerical Modelling of Terahertz Systems for Nondestructive Evaluation of Dielectric Structures. COMPEL - The International Journal for Computation and Mathematics in Electrical and Electronic Engineering 2013; 32 (3): 736–49, https://doi.org/10.1108/03321641311305719.
16. Majchrowicz M, Kapusta P, Jackowska-Strumiłło L, Sankowski D. Acceleration of image reconstruction process in the electrical capacitance tomography 3d in heterogeneous, multi-GPU system. Informatics Control Measurement in Economy and Environment Protection 2017; 7 (1): 37–41, https://doi.org/10.5604/01.3001.0010.4579.
17. Mikulka J. Accelerated Reconstruction of T2 Maps in Magnetic Resonance Imaging. Measurement Science Review 2015; 4: 210–18, https://doi.org/10.1515/msr-2015-0029.
18. Park S, Na J, Kim M, Lee J M. Multi-Objective Bayesian Optimization of Chemical Reactor Design Using Computational Fluid Dynamics. Computers & Chemical Engineering 2018; 119 : 25–37, https://doi.org/10.1016/j.compchemeng.2018.08.005.
19. Psuj G. Multi-Sensor Data Integration Using Deep Learning for Characterization of Defects in Steel Elements. Sensors 18 (2): 292, https://doi.org/10.3390/s18010292.
20. Romanowski A. Big Data-Driven Contextual Processing Methods for Electrical Capacitance Tomography. IEEE Transactions on Industrial Informatics 2018; 1–1, https://doi.org/10.1109/TII.2018.2855200.
21. Rymarczyk T, Adamkiewicz P, Polakowski K, Sikora J. Effective Ultrasound and Radio Tomography Imaging Algorithm for Two-Dimensional Problems. Przegląd Elektrotechniczny 2018; 94 (6): 62–69.
22. Rymarczyk T, Kłosowski G, Kozłowski E. A Non-Destructive System Based on Electrical Tomography and Machine Learning to Analyze the Moisture of Buildings. Sensors 2018; 18 (7): 2285.
23. Rymarczyk T, Kłosowski G. Application of Neural Reconstruction of Tomographic Images in the Problem of Reliability of Flood Protection Facilities. Eksploatacja i Niezawodnosc - Maintenance and Reliability 2018; 20 (3): 425–34, https://doi.org/10.17531/ein.2018.3.11.
24. Rymarczyk T, Sikora J. Applying Industrial Tomography to Control and Optimization Flow Systems. Open Physics 2018; 16 (1): 332–45, https://doi.org/10.1515/phys-2018-0046.
25. Sobaszek Ł, Gola A, Świć A. Predictive Scheduling as a Part of Intelligent Job Scheduling System: in, 358–67. Springer, Cham 2018, https://doi.org/10.1007/978-3-319-64465-3_35.
26. Soleimani M, Mitchell C N, Banasiak R, Wajman R, Adler A. Four-dimensional electrical capacitance tomography imaging using experimental data. Progress In Electromagnetics Research 2009; 90: 171–86, https://doi.org/10.2528/PIER09010202.
27. Tian G, Yang B, Dong M, Zhu R, Yin F, Zhao X, Wang Y, Xiao W, Wang Q, Zhang W. The Effect of Temperature on the Microbial Communities of Peak Biogas Production in Batch Biogas Reactors. Renewable Energy 2018; 123: 15–25,https://doi.org/10.1016/j.renene.2018.01.119.
28. Voutilainen A, Lehikoinen A, Vauhkonen M, Kaipio J P. Three-Dimensional Nonstationary Electrical Impedance Tomography with a Single Electrode Layer. Measurement Science and Technology 2010; 21 (3): 035107, https://doi.org/10.1088/0957-0233/21/3/035107.
29. Wang Mi. Industrial Tomography: Systems and Applications. Edited by Elsevier Ltd. Woodhead Publishing 2015.
30. Ziolkowski M, Gratkowski S, Zywica A R. Analytical and Numerical Models of the Magnetoacoustic Tomography with Magnetic Induction. COMPEL - The International Journal for Computation and Mathematics in Electrical and Electronic Engineering 2018; 37 (2): 538–48, https://doi.org/10.1108/COMPEL-12-2016-0530.

Tomasz RYMARCZYK
University of Economics and Innovation
ul. Projektowa 4, 20-209 Lublin, Poland
Research and Development Center, Netrix S.A.
ul. Związkowa 26, 20-148 Lublin, Poland

Grzegorz KŁOSOWSKI
Lublin University of Technology
Department of Organization of Enterprise
ul. Nadbystrzycka 38D, 20-618 Lublin, Poland

E-mails: tomasz@rymarczyk.com, g.klosowski@pollub.pl